Bulletin of the Seismological Society of America, Vol. 92, No. 7, pp. 2670–2688, October 2002

Three-Dimensional Excavation and Recent Rupture History along the Cholame Segment of the San Andreas Fault

by Jeri J. Young, J Ramón Arrowsmith, Laura Colini, Lisa B. Grant, and Brian Gootee

Abstract A paleoseismic study conducted along the Cholame segment of the San Andreas fault provides evidence for three earthquakes and the amount of lateral offset for the most recent event (1857 Fort Tejon earthquake). Excavations at the Las Yeguas (LY4) site include five fault-perpendicular, two parallel, and several hand-dug trenches. Abruptly truncated sand and silt layers that are not correlative across the fault zone constrain the timing of the penultimate event (L2) between cal. A.D. 1030–1300 and 1390–1460. Vertical offset, shearing, and fracturing of silty sand and gravel units that overlie L2 and historical artifacts that bracket the timing of the MRE (L1) provide evidence that the most recent ground-rupturing event, L1, occurred between cal. A.D. 1390–1460 and ~1865. L1 is likely the 1857 Fort Tejon earthquake. Tectonic silt-filled fractures that dissect historic gray-tan silt and sand suggest a ground shaking or a triggered slip event (L0), which occurred after L1. Three-dimensional excavation of an alluvial fan edge (unit 4) indicates that 3.0 ± 0.70 m of near-fault brittle slip occurred during the 1857 earthquake at this site.

Introduction

The Cholame segment of the San Andreas fault (SAF) lies between the partially creeping Parkfield (Bakun and Lindh, 1985) and locked Carrizo segments (Sieh, 1978) (Figs. 1, 2). The fortuitous location of this segment between the Parkfield and Carrizo segments allows it to record the interaction between these two segments with contrasting rupture behavior. Despite its potentially important role in elucidating the interface between these two diverse segments (Sieh and Jahns, 1984; WGCEP, 1988, 1995; Harris and Archuleta, 1988; Arrowsmith *et al.*, 1997), the earthquake history of the Cholame has been poorly studied (with the notable exception of Stone *et al.*, [2002]). In particular, event chronologies in this area are limited and vary between observers (Sieh, 1978; Lienkaemper and Sturm, 1989; Lienkaemper, 2001). Those studies that constrain the timing of ground rupture in the area are ambiguous and suggest the possibility of independent rupture of the Cholame and Parkfield segments after the last large earthquake that ruptured the Carrizo segment in 1857 (Stone *et al.*, 2002). Because the SAF in this area is thought to slip at a constant rate over several earthquake cycles, difference inferences of the fault slip in the area during the last earthquake lead to large discrepancies in the hazard the segment currently poses. Clearly, both paleoseismic excavation data that record the timing of events and offset data constraining their magnitude are necessary to formulate a meaningful seismic hazard evaluation of this seismically important section of the SAF.

To better constrain the earthquake history along this section of the SAF, we conducted a paleoseismic investigation along the central part of the Cholame segment near Las Yeguas Canyon (LY4 site). The site was chosen during the 1999 Stone *et al.* (2002) investigation because of its accessibility and apparently favorable depositional environment to record ground rupture. Seven major trenches and five radiocarbon ages provide evidence for and timing constraints of two ground-rupturing and one fracturing event. To constrain the offset magnitude at the site during the 1857 Fort Tejon event, we exhumed a displaced channel margin. Our data demonstrate that there has been no ground rupture in this area after 1857.

Figure 1. (A) Shaded relief map showing major faults in red and the location of the Las Yeguas study site. Important locations and the Parkfield and Cholame segments of the San Andreas fault (SAF) are indicated. Note that the Carrizo segment of the SAF is southeast of the Cholame segment. (B) Portion of the strip map along the central Cholame segment by Stone (1999). The map shows the location of the LY4 site and Figure 2 in the context of the fault traces, tectonic landforms, landslides, the basic geologic units, and the prior mapping of the area by Vedder and Wallace (1970). The LY4 site is situated on the central of three young alluvial fans (shown as Y on the map). Successively older fan and basin units are mapped as M1 and M2. The trench site is located in the southeast corner of Township 28, South Range 18, East Section 22.

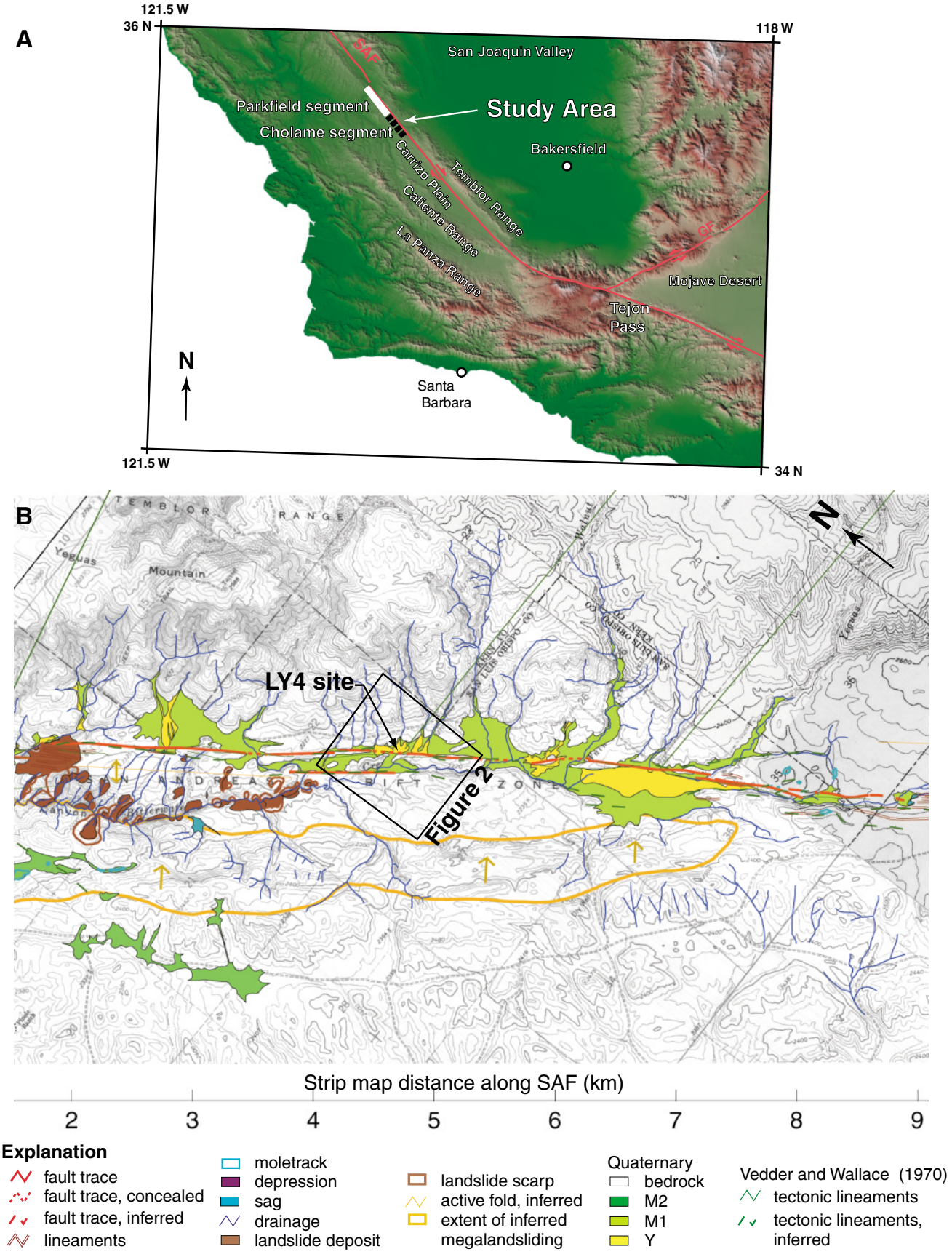
A
121.5 W
36 N
118 W
34 N
121.5 W
SAF
San Joaquin Valley
Parkfield segment
Cholame segment
Study Area
Bakersfield
Carrizo Plain
Temblor Range
Caliente Range
La Panza Range
GF
Mojave Desert
Tejon Pass
N
Santa Barbara
B
TEMBLOR RANGE
Yegua Mountain
N
LY4 site
Figure 2
SAN ANDREAS RIFT ZONE
Strip map distance along SAF (km)
2
3
4
5
6
7
8
9
Explanation
fault trace
fault trace, concealed
fault trace, inferred
lineaments
moletrack
depression
sag
drainage
landslide deposit
landslide scarp
active fold, inferred
extent of inferred megalandsliding
Quaternary
bedrock
M2
M1
Y
Vedder and Wallace (1970)
tectonic lineaments
tectonic lineaments, inferred

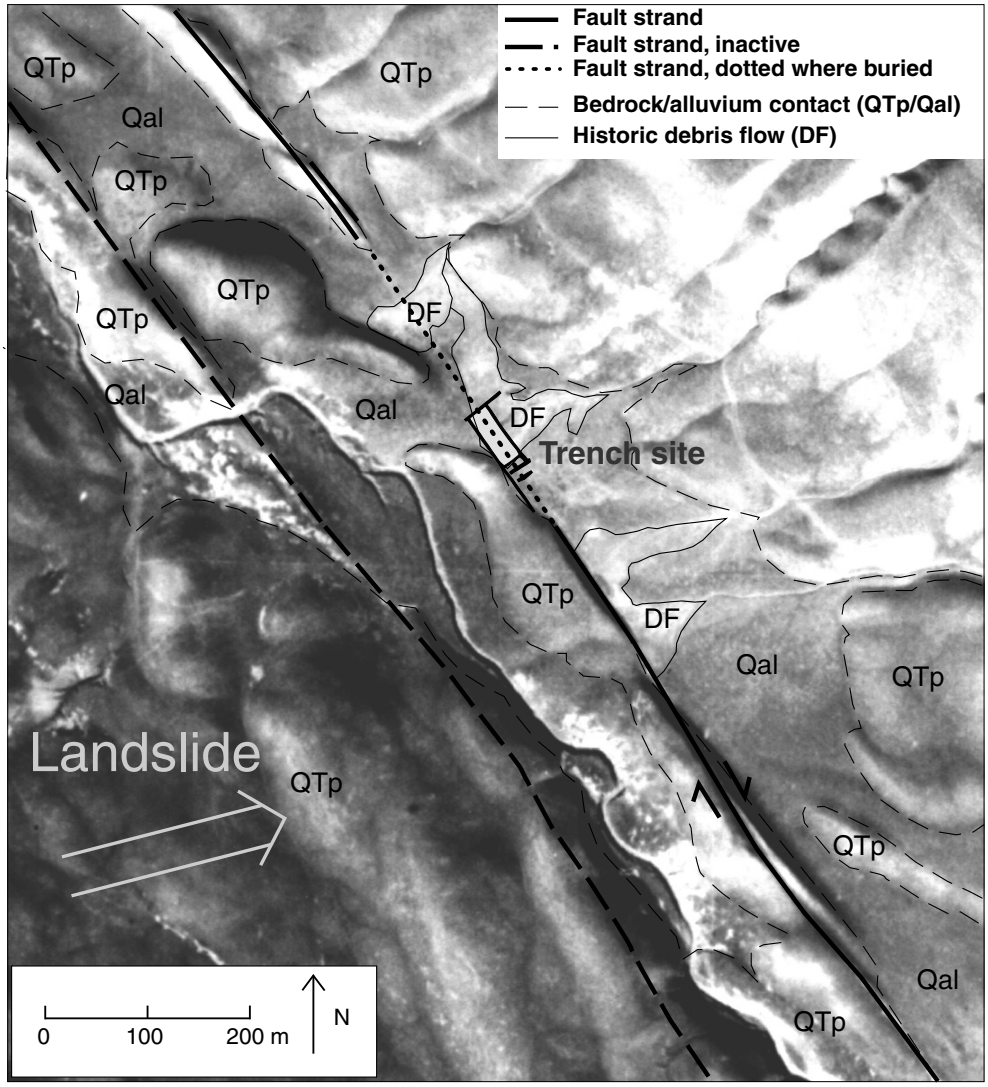

Figure 2. Aerial photograph of the LY4 earthquake geology site (courtesy of the Fairchild Aerial Photography Collection at Whittier College, Flight C-1260, taken in December, 1930) showing the locations of the active and recently inactive fault traces, major landforms, and the geologic units. The southwest fault trace has not been recently active as indicated by degraded fault scarps and undeformed inferred Holocene deposits (e.g., west-northwest of the trench site). Modified from Stone (1999).

In this article, we describe our geomorphologic and paleoseismic investigations at LY4. Significant stratigraphic units and their relation to earthquakes are described and used to interpret the timing of earthquakes at the site. In addition, three-dimensional excavations that constrain displacement along the fault during 1857 are described, and the significance of the measurements is evaluated. We discuss these new offset and timing constraints in the context of previous work and current hazard assessments. Finally, we examine the bearing of our data on the only other paleoseismic excavation study in the area (Stone *et al.*, 2002), specifically regarding their evidence for a post-1857 event.

Methods

Our paleoseismic study consisted of geomorphic characterization of the site, topographic surveys of relevant landforms, paleoseismic excavations, and radiocarbon age analysis. First, the fault-trace geometry and geomorphic units were mapped on ~1:6000 aerial photographs. Next, the site was surveyed with a Leica Total Station to characterize the topographic expression of the SAF (Fig. 3). Thirteen total paleoseismic excavations were performed at the site. In each of the trenches, the walls were shoveled, scraped, and brushed clean, and stratigraphic units were identified and marked with colored flagging. Physical descriptions of the

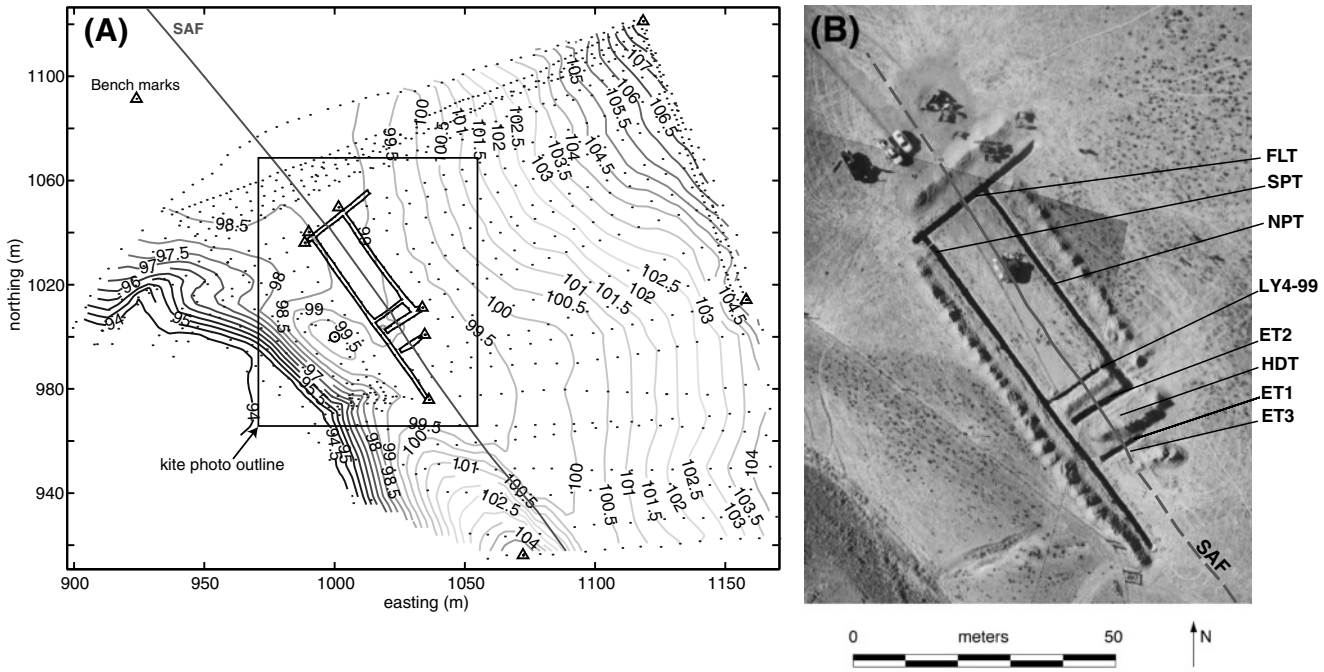

Figure 3. (A) Topographic map of the LY4 site. Note the position of the trenches on the distal portions of the alluvial fans emanating from the Temblor Range to the northeast. Trench outlines and the SAF are in black. Not all small HDTs are shown. Dots are surveyed points; triangles and circled location are local benchmarks. Contour interval is 0.5 m. The outline of B is shown by the box. (B) Rectified kite mosaic of the LY4 site showing the outline of the major trenches. The locations of the HDTs and ET3 are indicated, even though the photographs were taken before they were dug. These 100 m above the ground and warped to produce this mosaic using the surveyed data shown in A.

sediments were defined based on color, bedding thickness, texture, grain size, sorting, and other features such as degree of bioturbation. These units were then mapped using level lines as references at a scale of 1:10 for the fault-perpendicular trenches (FLT, ET1, ET2, ET3), 1:20 for the hand-dug trenches (HDT) and the reexcavated LY4-99 trench (Stone *et al.*, 2002), and 1:50 for the fault-parallel trenches (NPT and SPT). During and after mapping the trench walls, crosscutting relationships between strata, stratal mismatches, sediment thickness changes, shearing and tilting of strata, and fractures were used to deduce the relative sequence of ground-rupturing events. Letter names were assigned to each interpreted event (abbreviated L# for Las Yeguas events). One charcoal sample and one organic-rich sediment sample were collected and radiocarbon dated using accelerator mass spectrometry (AMS) ^{14}C dating methods (Beta Analytic) to provide age estimates for deposits and interpreted event horizons.

We reexcavated the fault-perpendicular trench from the previous study (Stone *et al.*, 2002) (trench LY4-99), added a fault perpendicular trench (FLT) 40 m to the northwest, and subsequently excavated three additional fault-perpendicular trenches (ETI–ET3) (Fig. 3). FLT was excavated to provide a more accurate location of the fault where geomorphic expression is poor (Fig. 2). ET1 and ET2 were excavated to further constrain the timing of events at the site. To constrain lateral offset of subsurface deposits, fault-parallel trenches (NPT and SPT) were excavated ~7 m on either side of the SAF (Figs. 2, 3). Two fault-perpendicular trenches were excavated for event timing (ET1 and ET2). Several hand-dug trenches were excavated (labeled as HDT1-7) to expose the edge of a buried alluvial fan offset by the fault during the last ground-rupturing event. Finally, a 5 m × 1.5 m surface excavation was performed to expose tectonic fractures initially identified in ET1. A shallow HDT (ET3) was excavated to expose the upper 1.5 m of sediment to determine any post-1857 offset (Stone *et al.*, 2002).

Results

Site Description

LY4 is located on an alluvial fan whose distal edge crosses the SAF (Figs. 2, 3). The provenance for the Holocene fan sediments at the site includes the nonmarine Pleistocene Paso Robles Formation, the marine Miocene Monterey Formation, and the marine Oligocene–Miocene Temblor Formation exposed in the surrounding hills (Dibblee, 1973). The Paso Robles Formation is composed mainly of sand, silt, and clays that were derived from the older Mon-

terey and Temblor Formations. The Monterey Formation is characterized by interbedded marine sediments, such as siliceous siltstones, shales, porcelainites, and sandstones. Nonmarine sandstones, shales, and conglomerates make up the Temblor Formation.

Recent fan deposition obscures the surface expression of the SAF in the immediate area of the trenches. However, the surface trace of the SAF is defined by linear fault scarps and less prominent geomorphic lineaments to the southeast and northwest of the site, respectively. Approximately 200 m southeast of our excavations, the fault cuts the edge of a northwest–southeast trending hill, continues northwest along the base of the hill, and is finally obscured by recent deposition ~50 m southeast of the excavations. The fault truncates several alluvial fans approximately 175 m northwest of our trenches; however, the geomorphic expression of the fault is less pronounced here than southwest of the site (Fig. 2). Further northwest, relatively steep scarps delineate the recently active trace of the fault. Another fault trace exists west our excavation site (Fig. 2); however, both Stone *et al.* (2002) and our study interpret this trace to be inactive because it has a degraded surficial expression and does not offset inferred Holocene landforms.

Fault Zone Stratigraphy

Stratigraphic units were identified and described in each trench for intertrench and intratrench correlation. Sediments are derived from clays and fine-grained marine and nonmarine rocks of the Monterey and Temblor Formations, respectively. Because primary clay content of the sediments at the LY4 site is difficult to differentiate from secondary pedogenic clay content, soil classification is limited. The color of the sediment is generally tan-tan-gray with no apparent rubification. Lithologic contrasts are well preserved across the fault in ET1, ET2, ET3, and fault-perpendicular hand-dug trenches (HDTs). ET1 is characterized by bedded sand and silt surrounded above and below by bioturbated, clayey, sandy silt on both sides of the fault (Figs. 4, 5). In contrast, the strata exposed on the southwestern side of the fault in trench ET2 generally lacks bedding, are densely bioturbated and moderately to heavily fractured, and are composed of clayey, sandy silt (Fig. 6). On the northeast side of the fault, the strata in ET2 exposed contrasting layers of coarse clastic deposits and clayey, sandy silt. Like ET1, trenches ET3 and HDT expose bedded sand and silt surrounded by bioturbated silt (Figs. 7–9). Below, we describe important stratigraphic units and interpret the depositional history of each unit. Generally, units are numbered in ascending order from the relatively youngest to oldest units; where units were subdivided, letters were assigned in ascending order according to age.

Important Units on the Northeastern Side of the Fault. The oldest significant stratigraphic units on the northeastern side of the SAF are laminated silt, sand, and gravel of units 13, 12, and 11, respectively, found in ET2 (Fig. 6). Unit 13 is a medium-tan, very fine sandy, clayey silt with laminated organic silts near the top of the unit. Units 12 and 11 are interpreted as fluvial deposits of laminated silts and sands (unit 12) overlain by debris flow deposits of coarse angular sand and gravel (unit 11) (Fig. 6). Unit 9 is composed of light beige to tan, very fine sandy, clayey silt. ET1, ET2, ET3, and HDT expose units 4 and 5; the latter stratum is a distinct marker bed throughout much of the site. It is composed of tan-beige laminated silt and fine sand and interbedded clayey silt and fine pebble stringers. In ET1, ET3, and parts of HTD, unit 4 is comprised of a tan, crudely imbricated angular, medium- to coarse-grained sand. It also contains very fine pebble-size clasts that are crudely oriented parallel to bedding. It fines upward but coarsens laterally to the northeast toward ET2. In this trench, unit 4 is characterized by angular gravel with lenses of coarse sand near the base and top (unit 2c) of the unit (Fig. 6). The contact between unit 5 and unit 4 appears to be gradational. Fine pebble stringers and coarse sand of unit 5 pinch into the overlying coarse sand of unit 4 in ET1 and gravel of unit 4 in ET2 and the northern parallel trench. Unit 2c is composed of light tan-beige, angular to subrounded, fine silt to fine- and medium-grained sand with crude layering at its base. It is moderately bioturbated, thins laterally, and is only present on the northeast side of the SAF zone; however, overlying unit $2b_1$ is identifiable on both sides of the fault zone. This unit is composed of orange-brown silty sand to sandy silt and is disseminated in places (Figs. 4–9). A 0.5- to 2.5-cm-thick organic-rich silt (unit 2a) is observed in all trench exposures and has developed on top of the last well-developed soil, unit 2b. Unit 2a is a dark gray, carbonaceous, fine sandy, clayey silt. It is exposed on both sides of the fault throughout the entire trench site and contains historic anthropogenic debris such as squared-tipped nails, white porcelain, lumber, rusted tin, and blue-washed glass. Some of these historic artifacts also are present within unit 2b. Beige, well-bedded, very fine to very coarse sand, and silt comprise the upper 30 to 35 cm of overlying sediments throughout the site (units 1a, b, c, and d).

The fine laminations within unit 12 and unit 5 silts and sands indicate suspensate settling from a single hydrodynamic depositional event. Ponding or low energy associated with lag waters from a meandering fluvial environment are compatible with the fine laminae and fine grain sizes of units 12 and 5. Ponding may have occurred against or slightly over a preexisting fault scarp because unit 5 thins rapidly across the fault zone. Alternatively, the thinning may be a result of both depositional thinning and the juxtaposition of a thinner and thicker portion of the unit due to lateral offset. Unit 4 has undergone a facies change from medium to coarse sand to fine cobble gravel in the 7 m separating ET1 from ET2 (Fig. 3). The angularity, submaturity, and poorly sorted texture of the coarse sand facies of unit 4 are suggestive of low to moderate depositional energy such as that of a distal alluvial or debris fan deposit. Crude imbrication of gravels from units 4 and 11 indicate a northeast to easterly source

that is consistent with modern alluvial fan development (Figs. 2, 3). The angularity, poorly sorted nature, and submature texture of this deposit suggests low transport energy typical of debris flow deposits. Rapid thinning of unit 4 may be explained by deposition across the fault over a preexisting scarp. The facts that unit 4 is gradational between gravel and coarse sand, consistently overlies marker unit 5, and is interpreted to be an alluvial fan deposit imply that the gravel in ET2 and the sand from ET1 were coevally deposited. The organic-rich silt, unit 2a, resulted from continual surface exposure and accumulation of organic debris on top of tan-gray silt unit 2b. Nonlayered sediments, such as unit 2b, can generally be classified as B (pedogenic) horizons, and unit 2a can be described as a modern A horizon. Fine-grained layered silts such as units 5 and 13 are likely preserved because they are overlain by gravel and coarse sand, which may have protected them from bioturbation. Although some of the sedimentary horizons have been bioturbated, correlative units remain identifiable from trench to trench (Fig. 10).

Important units found only on the southwestern side of the fault zone include units 18 and 17 in ET2 and units 8b and 7b in ET1. Unit 18 is the oldest layered unit at the site and is composed of beige, fine sandy silt and sand interbeds. This unit is cut by a 2.5-cm thick, 2-m-long, vertical silt-filled tectonic fracture in both walls of ET2. Unit 17 is a mediums to coarse-grained sand that is disseminated in places due to bioturbation (Fig. 6). Unit 7b is a very fine sandy silt that has been moderately bioturbated (Fig. 4) and extensively fractured (Fig. 4). Unit 8b is slightly coarser than 7b but has many of the same features of 7b (Figs. 4, 6).

Estimating Ages of Stratigraphic Units. The limited carbon production and preservation at the LY4 site has resulted in few samples suitable for dating; thus we were able to date only two during this study (Table 1). Both were collected from northeast of the fault in ET2, from the southeast and northwest walls. Sample number LY4-00-1 was collected from carbon-rich silt at the top of unit 13 and processed as a bulk sediment sample to yield a 2σ calibrated age of cal. 80 B.C. to cal. A.D. 80. We acknowledge that age estimates associated with dating bulk organic matter from soil have much larger uncertainties than reported analytical uncertainty for the resulting ^{14}C age because organic matter in cumulic soils may have a mixture of materials of different ages, ranging from modern to several thousands of years old (Trumbore, 2000).

Sample number LY4-00-3, from laminated silt unit 5, was processed as charred wood and yielded a 2σ calibrated age of cal A.D. 1390–1460 (Table 1). This calibrated age seems reasonable for unit 5 because the sample dated was not a bulk sample and is younger than the ages obtained for underlying unit 13 (see below) and because the rate of deposition for sediments above the sample location is consistent with that made from the historic sediments. Because this is the only date obtained from unit 5, it must be considered a maximum age for this deposit. More dates would be necessary to determine if this sample was detrital in origin and significantly older than the deposit.

Stone *et al.* (2002) obtained two dates on detrital charcoal from unit 13 (their unit 40). Both samples yield an age of 1030–1300 A.D. Their age estimate is more reasonable than our age estimate of this unit for three reasons: (1) Stone *et al.* (2002) samples were detrital charcoal rather than bulk sediment; (2) depositional rates that can be estimated from the thickness of the historic sediments and their age (about 0.20–0.30 cm/yr) are not consistent with the thickness of sediments overlying unit 13, assuming an old age for the unit, and (3) the 2000-year-old estimate from this study is excessively old compared to the preservation of young sedimentologic features, such as the nonbioturbated bedding plane preservation of unit 13 and lack of extensive soil development (Fig. 6).

The historic anthropogenic debris collected from and directly below unit 2a indicates a post-1865 date for this unit and overlying sediments (units 1a–d). According to ranching families who have lived in the area for over 125 years, homesteaders did not occupy the Las Yeguas canyon area until the late 1860s (J. Cooper, 2001, personal comm.; D. Twisselman, 2000, personal comm.). The first group of homesteaders settled in the northern Carrizo Plain from 1865 to 1885 (Eichel, 1971), and the introduction of historical artifacts occurred sometime after 1865. The age of unit 2a may be older than the 1860 estimate because the anthropogenic debris may have been impregnated into an already exposed surface and is not *in situ*. Trampling and burrowing on or near an exposed substrate may vertically move debris into the soil column (Wood and Johnson, 1978). The overlying sediments (units 1a–d), however, are clearly less than 140 years old.

Description and Timing of Events

Event L2

Tectonic features of L2 truncate fine- and coarse-grained deposits in the lower halves ET1 and ET2. In ET1, units 7 and 8 southwest of the fault are truncated and fractured. Both units are rotated into the fault zone and do not cross the fault (Fig. 4). In ET1, fragmented lenses of sand (unit 6b) on the northeast side of the fault were not observed on the southwest side of the fault zone. In ET2, units 17 and 18 on the west side of the fault zone are truncated and fractured. The faulting of these three units is interpreted as the as one single event (L2) event because it occurred before the deposition of overlying units 4 and 5, but it may be the result of more than one earthquake. For example, a set of ~2.5-cm-wide, silt-filled fractures cut units 17 and 18 and terminate within the densely bioturbated clayey sandy siit below unit 5. Units 10–16 and 20 on the east side of the fault are not correlative with any units across the fault in ET2. In both walls, a 20- to 30-cm-wide wedge of gravel from unit 11 is vertically displaced and separated from the main body of the deposit

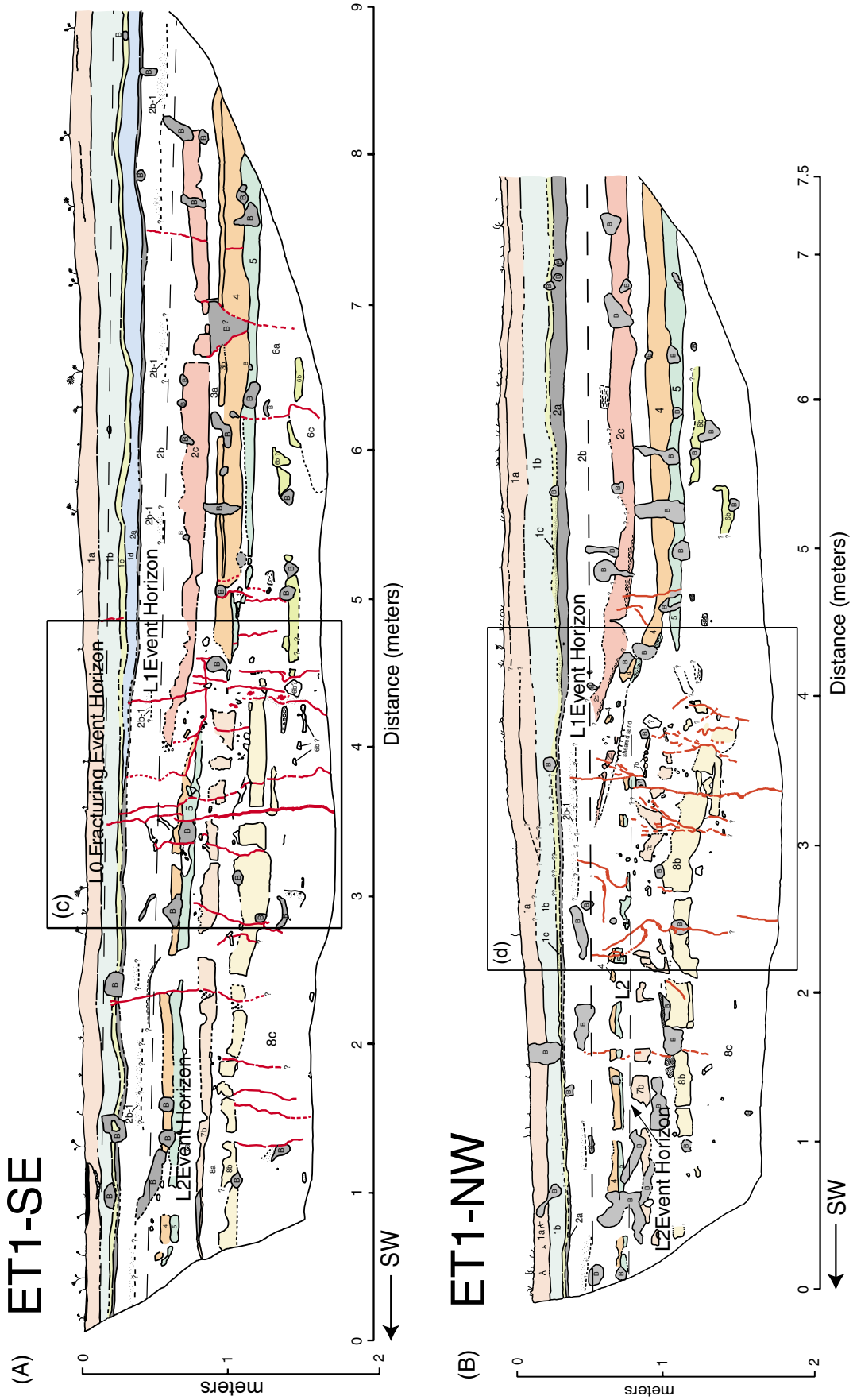
(A) ET1-SE
(c)
L0 Fracturing Event Horizon
L1Event Horizon
L2Event Horizon
meters
Distance (meters)
SW
(B) ET1-NW
(d)
L1Event Horizon
L2
L2Event Horizon
meters
Distance (meters)
SW

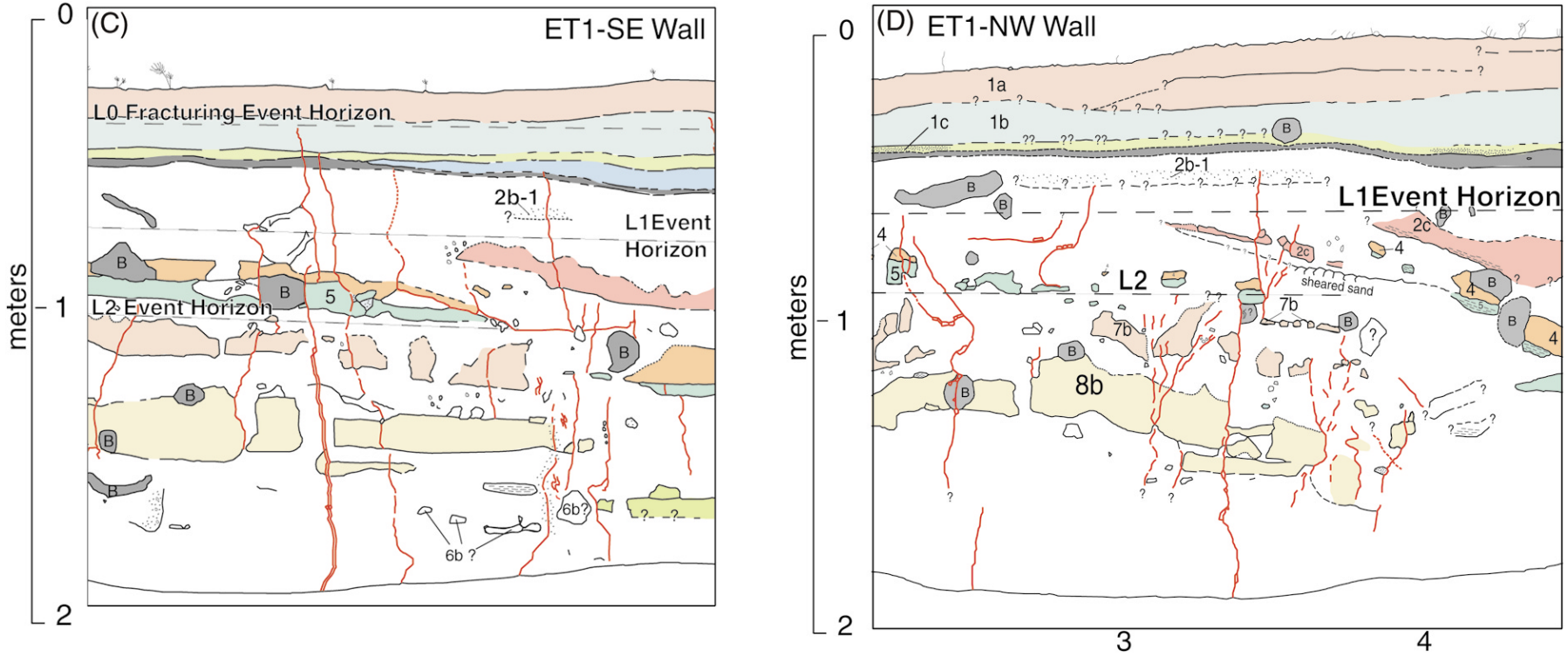

Figure 4. Trench logs of ET1: (A) southeast and (B) northwest walls. See Figure 3 for location. The stratigraphy is more bioturbated at depth on the southwest side of the logs, whereas the northeast side preserved alternating layers of coarse clastic deposits and clayey, sandy silt. (C) Blow up of ET1-SE and (D) blow up of ET1-NW (see parts A and B for location). Three earthquake event horizons, L1–L2 and one ground-shaking event, are indicated. L0 is above historic fracturing; L1 is above offset sandy unit 2c, L2 offset, and fractured units 4 and 5; L2 is above truncated and fractured unit 7. See Figure 5 for explanation of symbols and units.

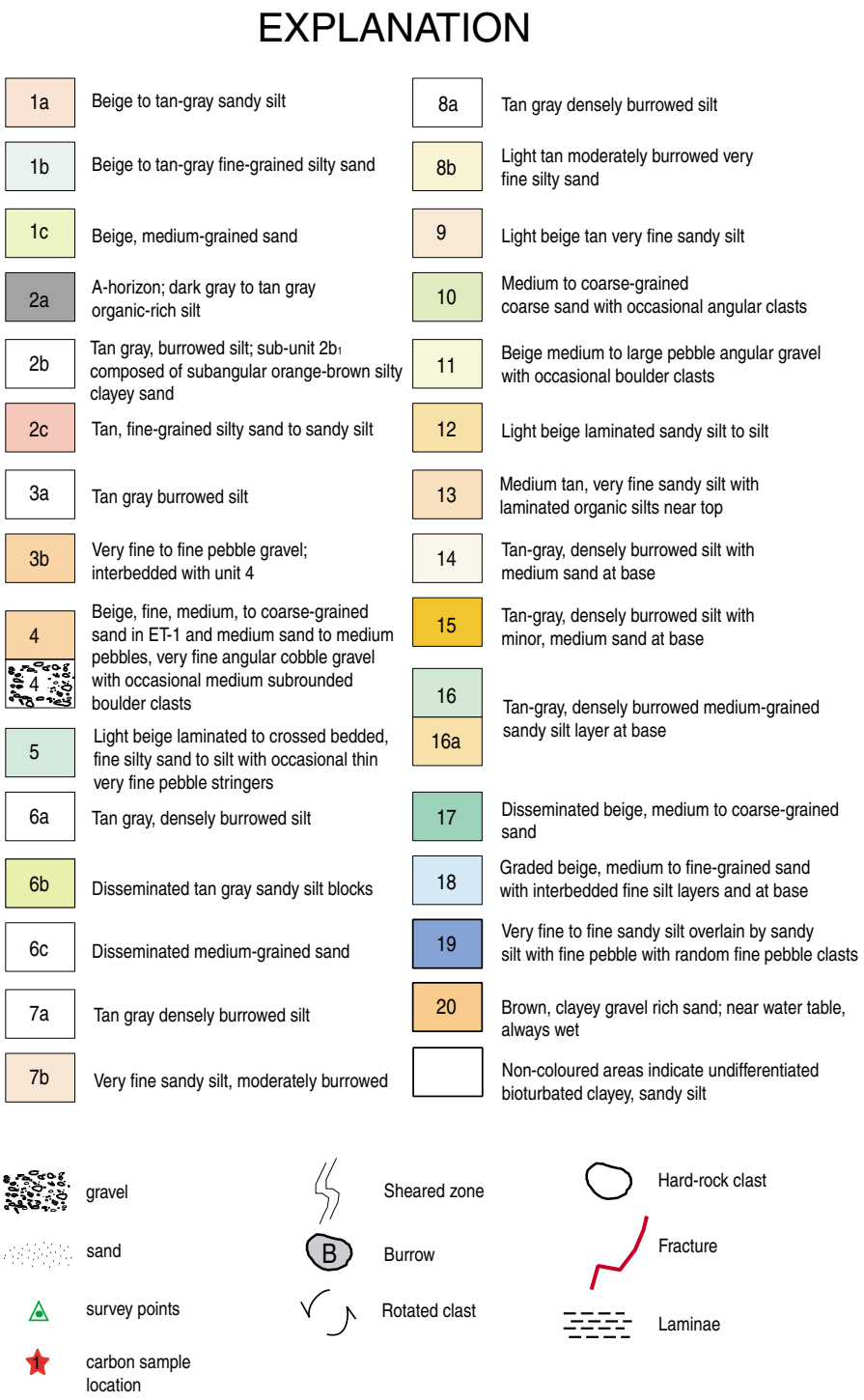

Figure 5. Explanation to accompany trench logs. Unit numbers were assigned from youngest to oldest in individual trenches, but unit numbers do not necessarily indicate unit ages from trench to trench. For example, unit 9 in ET2 may or may not be older than unit 7 from ET1, although numbers assigned to a unit in one trench is repeated in the second trench if the units are correlative.

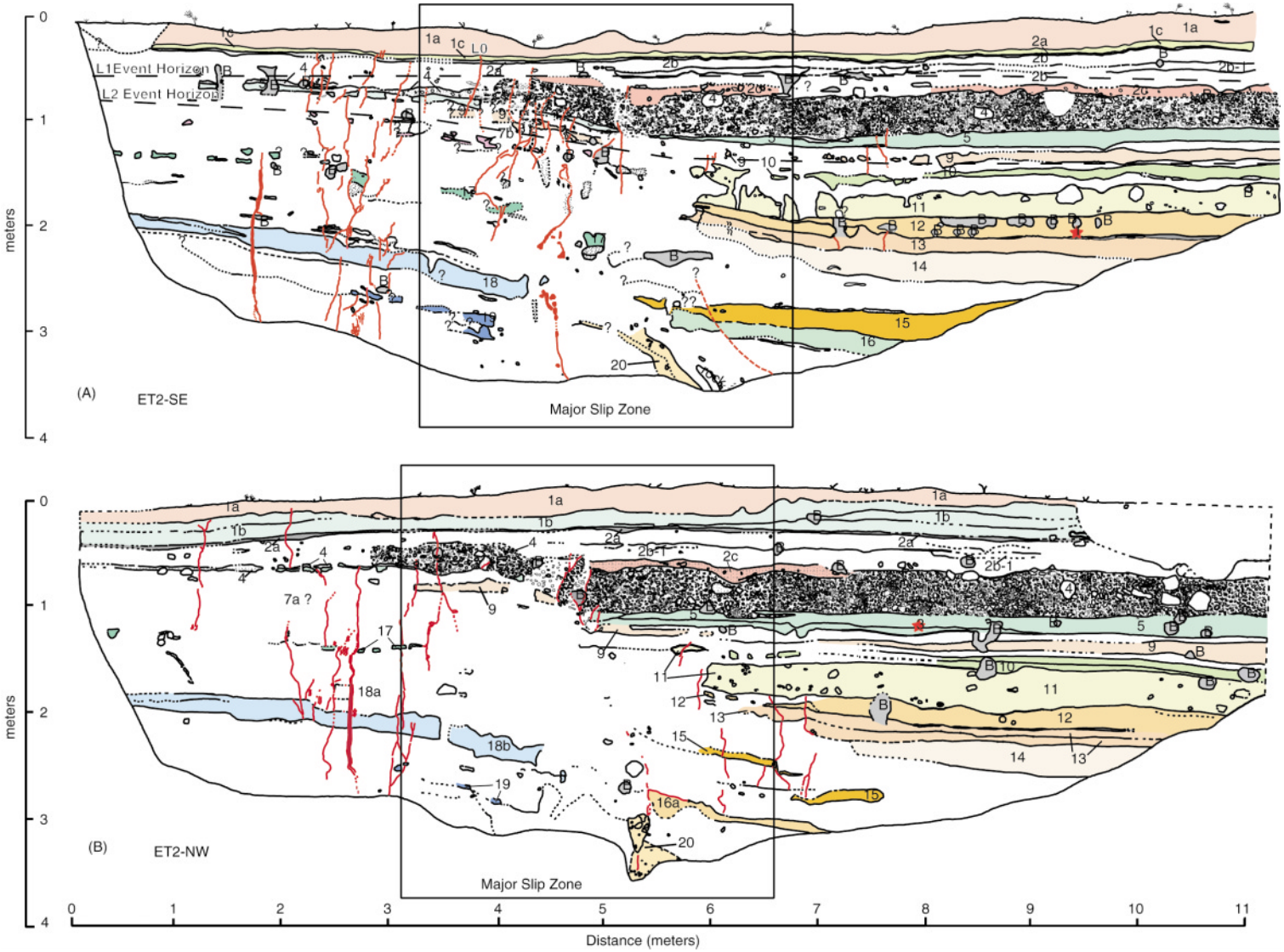

Figure 6. Logs of ET2: (A) southeast and (B) northwest walls. Although this excavation is deeper than ET1 (Fig. 4), the stratigraphic relations are similar. The more bioturbated stratigraphy on the southwest side of the logs is more evident, whereas the northeast shows alternating layers of coarse clastic deposits and clayey, sandy silt with the oldest units at the bottom indicating moderate dip. Unit 4 is much coarser in ET2 than in ET1. Three inferred earthquake event horizons, L2–L0, are plotted above truncated unit 9, separated and fractured unit 4, and fractured unit 2c, respectively. We do not define any additional older earthquakes despite the apparently greater deformation of unit 20 because we could not correlate it with nearby units.

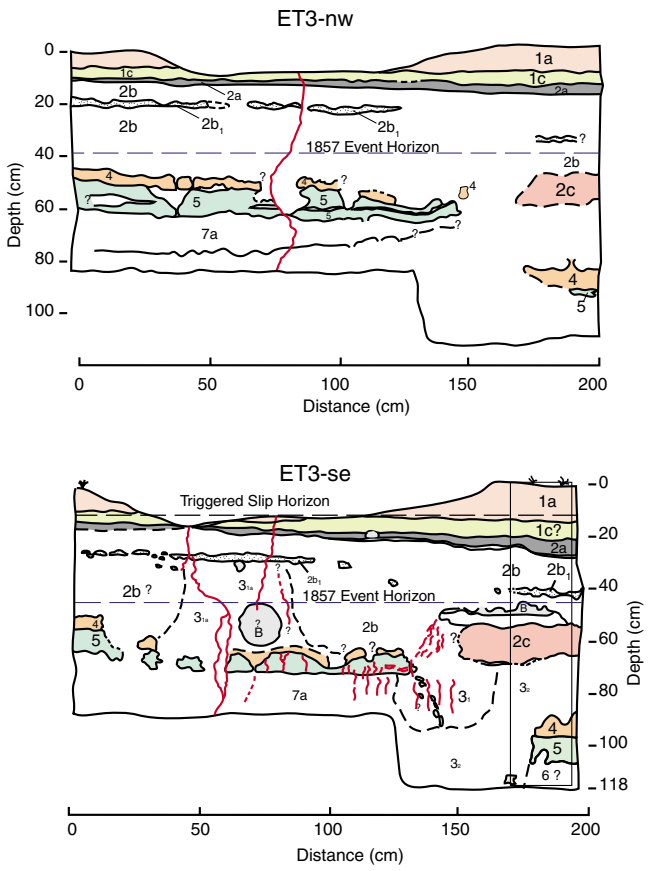

Figure 7. Trench log of ET3. See Figure 3 for location. The stratigraphy of ET3 is similar to that of upper portion of ET1 (Figs. 3, 4). Event horizons are indicated. Rectangle on the right side of ET3-SE is the location of the stratigraphic column shown in Figure 10. See text for discussion.

(Fig. 6A). The L2 event occurred sometime after the deposition of unit 11, before the deposition of unit 9 in ET2 (Fig. 6), after the deposition of unit 7, and before the deposition of unit 5 in ET1 (Fig. 4). Only units 5 and younger are correlative among the fault-perpendicular trenches.

The age of L2 is constrained by the three acceptable radiocarbon dates obtained from the trenches. It occurred after deposition of unit 13 and prior to the deposition of unit 5. The lower- and upper-bounding age constraints are from unit 13 and unit 5, bracketing the event between A.D. 1050 and 1460 (Table 1).

Event L1

L1 vertically displaced, separated, and sheared units 4 and 5, and most likely units 2b, $2b_1$, and 2c (Table 2). Units 4 and 5 have a maximum vertical displacement of 30–35 cm in both walls of ET1 and ET2. It is nuclear whether a small component of oblique slip along the SAF or the offset of an older bedform is responsible for the apparent offset. The sand and gravel clasts of unit 4 are rotated and heavily fractured in the fault zone. Laminated silt unit 5 is also heavily fractured and sheared. Minor amounts of gravel and sand from overlying unit 4 in-fill fractures within unit 5 (Fig. 4C). Both units cross the fault zone, although the abrupt gravel edge of unit 4 is only approximately 1 m away from the main fault zone (Fig. 6). Units 2b, $2b_1$, and unit 2c in ET1, ET2, and ET3 are fractured and vertically offset. The amount of vertical displacement of these units is less than that of units 4 and 5. This could result from sediment filling in a preexisting depression adjacent to a fault scarp on the southwest side of the fault zone. The units toward the top of this topographic low would have less relief or a shallower dip from the bottom of the individual layers to the top (Fig. 10). Surface rupturing event L1 occurred sometime after the deposition of unit 5, therefore sometime after A.D. 1390 but before the historic settlement years of the 1860s. Event L1 is likely the 1857 Fort Tejon Earthquake because offset and fractures from this event are proximal to the historic sediments.

Ground-Fracturing Event L0

Tectonic fractures designated L0 cut historic unit 2a and overlying historic sediments in ET1 and ET3 (Figs. 4A–D, 7, 11). Silt-filled sets of fractures are 2 cm and 1.5 cm wide at the bottom of ET3 and ET1, respectively, and thin to 0.5 cm at their termination in historic sediments toward the top of the exposed surfaces. In both trenches, elongate coarse sand particles are rotated with their long axes parallel to the fractures. Historic fractures in ET3 have a 322° strike. The orientation of the plane connecting the same fractures in ET1 is 354° at the bottom of the trench and 322° near the top of the trench. A morphologically similar set of silt-filled fractures in adjacent trench ET2 has the same orientations with respect to depth, although these fractures do not dissect historic sediments.

The termination of the most prominent silt-filled fractures of the southeast wall of ET1 and both wall of ET3 were excavated on a horizontal surface about 12 cm below the ground surface for 5 m by 2.5 m (Fig. 11). In map view, the fracture trace retained its silt-filled morphology, made several steps, and continued for the extent of the excavation. Three microtrenches were dug perpendicular to the fractures to verify their through-going nature. The repeating orientations of fractures in three different trenches and along the ground surface indicates that they were generated by a tectonic mechanism and probably are not the product of desiccation. One other explanation may be that a tectonic fracture associated with event L1 or L2 provided a plane of weakness for soil contraction, therefore propagating the fracture through modern sediments. Soil cracking is not found outside of the main fault zone and so it is not common at the site.

The source of these fractures could be from triggered slip associated with stress transfer from a Parkfield or other nearby earthquake or aseismic creep that occurred prior to modern creep measurements. Slip associated with the 1966 Parkfield earthquake extended at least 6 km south of High-

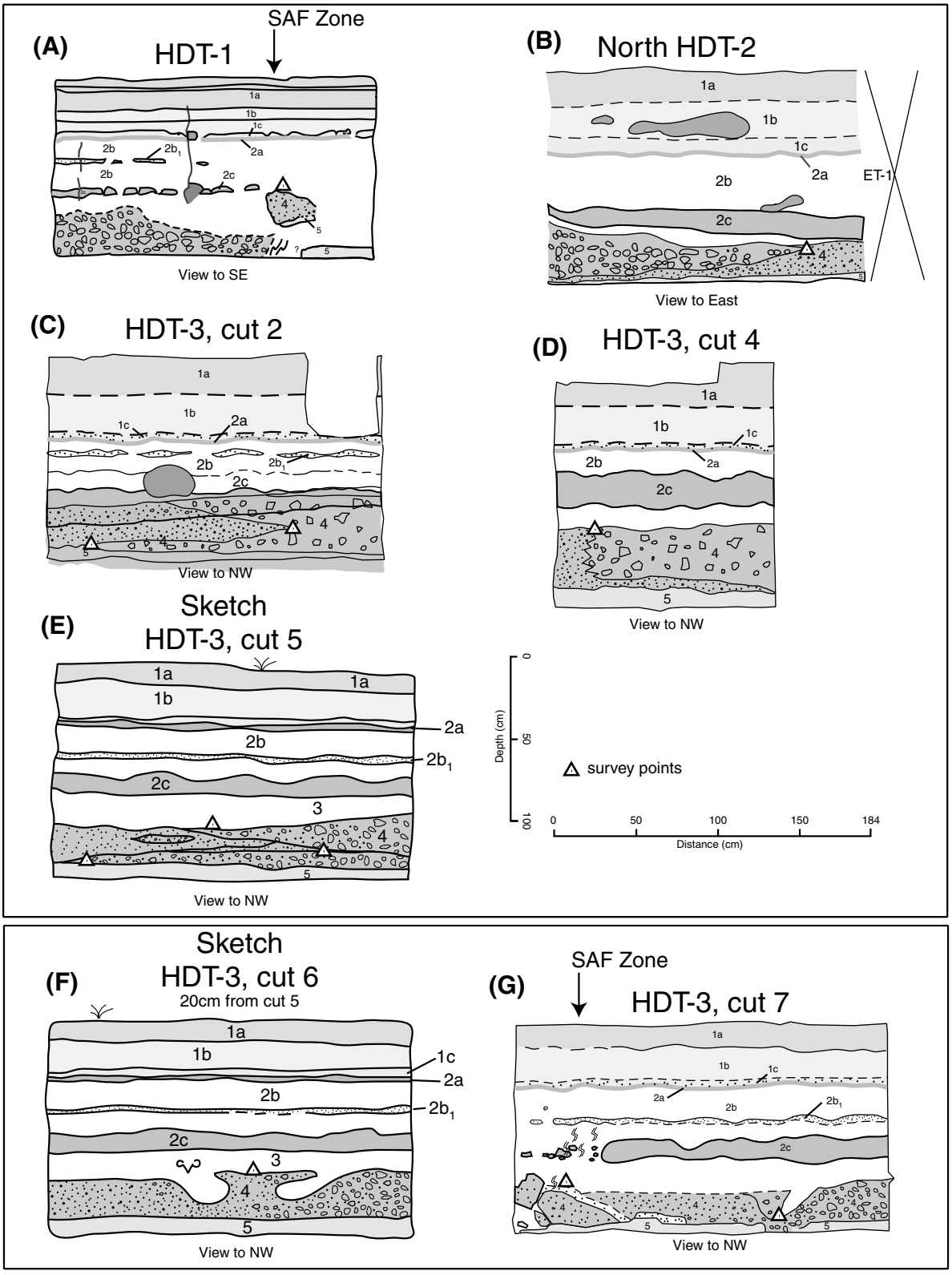

Figure 8. HDT logs mapped at 1:20 scale. Three initial trenches were modified by continually shaving the trench walls. See Figure 12 for locations of these logs. They sequentially depict the gravel edge and show how it varies from interfingering (cut 2) to gradational (cut 6) to abrupt (cut 4). The triangle marks the gravel edge that was surveyed and is shown in Figure 12.

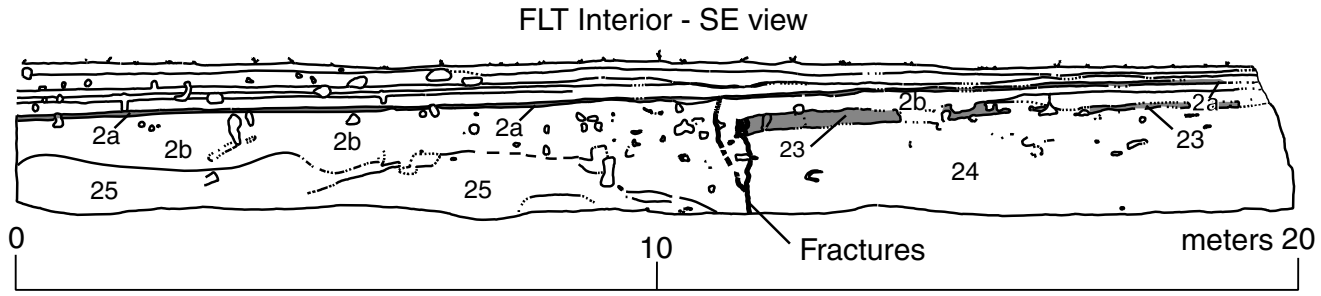

Figure 9. Trench log for the fault location trench southeast wall (FLT) see Figure 3 for location. The fault zone is indicated in heavier lines. Most of the lower portions of the stratigraphy are heavily bioturbated and generally correlated with older units across the site. The distinctive unit 2a was first observed in this trench, and historic artifacts were prominent within it on the southwestern portion of this wall.

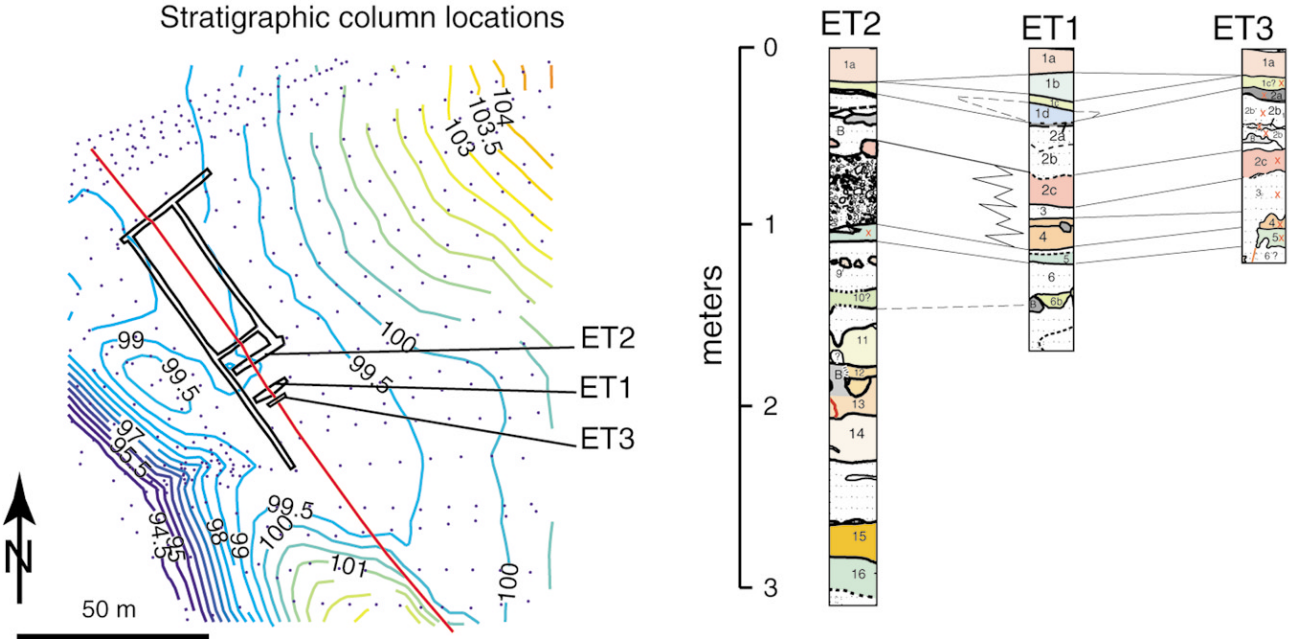

Figure 10. Stratigraphic columns used for unit correlation for fault perpendicular trenches ET1, ET2, and ET3. Location of each column is identified on the clipped topographic insert. Important unit correlations include unit 2c, $2b_1$, and 2a.

way 46 (Lienkaemper and Prescott, 1989), and it is reasonable that triggered slip from an older Parkfield earthquake such as the 1877 (T. Toppozada, personal comm., 2001) or the 1881 earthquakes may have occurred along the adjacent Cholame segment. Because of the unevenness of unit 2a, the amount of offset along the fractures is difficult to discern. Field measurements preclude a possible 0.5-cm estimate of vertical slip along the fractures, but horizontal displacement could not be estimated.

Three-Dimensional Paleoseismic Analysis

The oblique contact between the distal edge of an alluvial fan deposit (unit 4) and the SAF provide piercing points for determining the amount of lateral displacement after its deposition (Fig. 12). The upper surface and southern edge of unit 4 was excavated across the SAF between ET1 and ET2 to measure the amount of lateral offset of this unit.

Description of Fault Zone and Stratigraphy in the Hand-Dug Trenches

Several small trenches were excavated by hand to expose the edge and top surface of the gravel facies of unit 4 and the San Andreas fault between trenches ET1 and ET2. There are three main HDTs that we extended in a series of cuts approximately 10, 25, or 50 cm in between the fault-perpendicular trenches. Two of the HTDs were together to

Table 1
Radiocarbon Ages from the Las Yeguas Site: Years 1999 and 2000

Sample*	Unit§	Description	$^{13}C/^{12}C$	Conventional Age‖	2σ (95.4%) Calibrated Age Range#
LY4-00-1†	13	Bulk sediment from paleosol	−24.3	2000 ± 40 B.P.	110 B.C.–A.D. 90 (93.8%) A.D. 100–120 (1.6%)
LY4-00-3†	5	Charred wood	−25.1	480 ± 40 B.P.	A.D. 1330–1350 (2%) A.D. 1390–1490 (93.4%)
LY4-99-2‡	13 (35)	Charcoal fragment	−25.0	810 ± 50 B.P.	A.D. 1040–1090 (4.2%) A.D. 1120–1140 (2.7%) A.D. 1150–1300 (88.5%)
LY4-99-5‡	13 (35)	Charcoal fragment	−25.0	840 ± 60 B.P.	A.D. 1030–1290
LY4-99-31a†	5 (75)	Composite charcoal from paleosol	−25.0	2680 ± 60 B.P.	1000–760 B.C.

*See trench logs for sample locations.
†AMS date from Beta Analytic.
‡AMS date from Lawrence Livermore National Laboratories.
§Numbers in parentheses refer to numbering scheme of Stone *et al.* (2002).
‖B.P. is years before A.D. 1950.
#Calibrations were performed using OxCal Program v3.5 (Ramsey, 1995). Calibrated age ranges are illustrated in Figure 15.

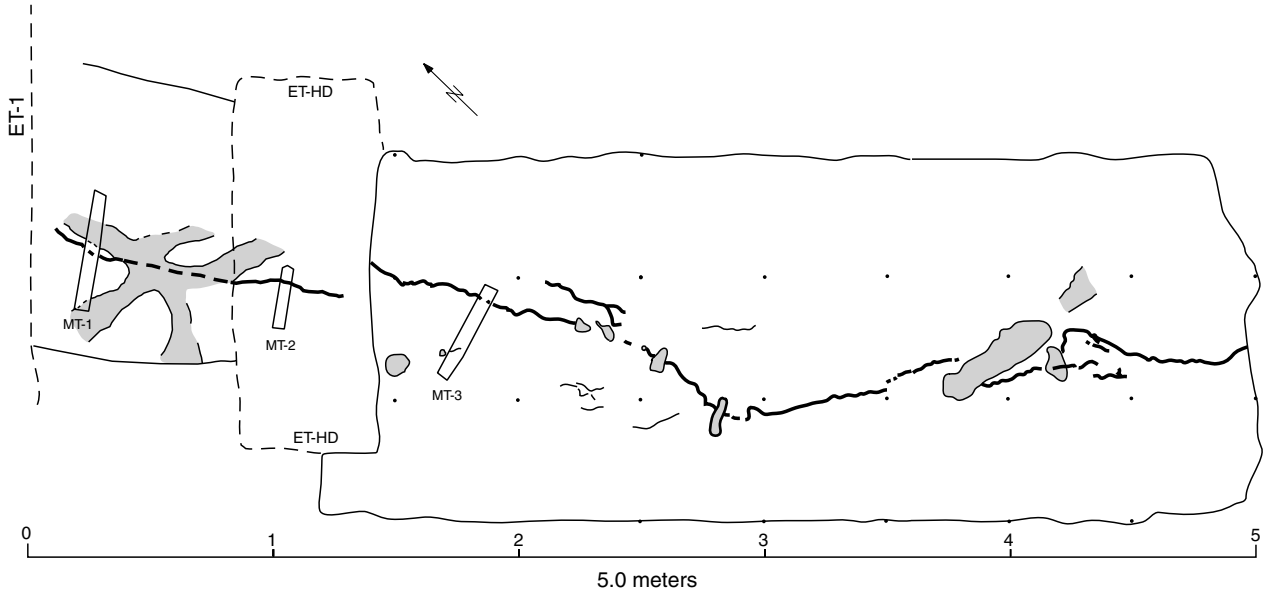

Figure 11. Silt-filled fracture of ET1-SE surface excavation; note burrow outlines in gray and microtrenches (MTs) in which the fractures were evident. The silt-filled fractures were discontinuous but localized in the center of this cleared zone immediately above the major fault zone exposed in the adjacent trenches (ET1,—see Fig. 4; ET3,—see Fig. 7). Opening of the fractures varies from a few mm to 1 cm. No clear evidence of offset—only opening—was preserved along them.

fully expose the edge and surface of the alluvial deposit (Fig. 8).

Units exposed in the HDTs include: 5, 4, 2b, $2b_1$, 2c, 2a, and 1a–c (Fig. 8A–G). Laminated silts of unit 5 provide a stratigraphic marker for determining the depth and extent of the alluvial fan unit 4. Unit 5 was consistently located at about 1.3- to 1.5-m depth and was highly sheared and broken in the fault zone. The characteristic bedding and fine-grain size of unit 5 made faulting of this unit more pronounced than in overlying coarse sediments, thus making this unit important in locating the main fault zone and a subsidiary fracture during the three-dimensional excavation. Unit 4 is composed of fine pebble to boulder size gravel and medium to coarse angular silty sand. The coarse angular pebble gravel of unit 4 in ET2 is not present in ET1, and there is coarse angular silty sand at the same stratigraphic horizon in ET1. The contact between an angular coarse pebble to fine cobble gravel and fine tan silt represents the outer edge of the alluvial fan. A previously existing fault scarp may have provided a topographic high that absorbed depositional energy associated with debris flow unit 4. The sudden drop in energy could have resulted in a spillover effect and conse-

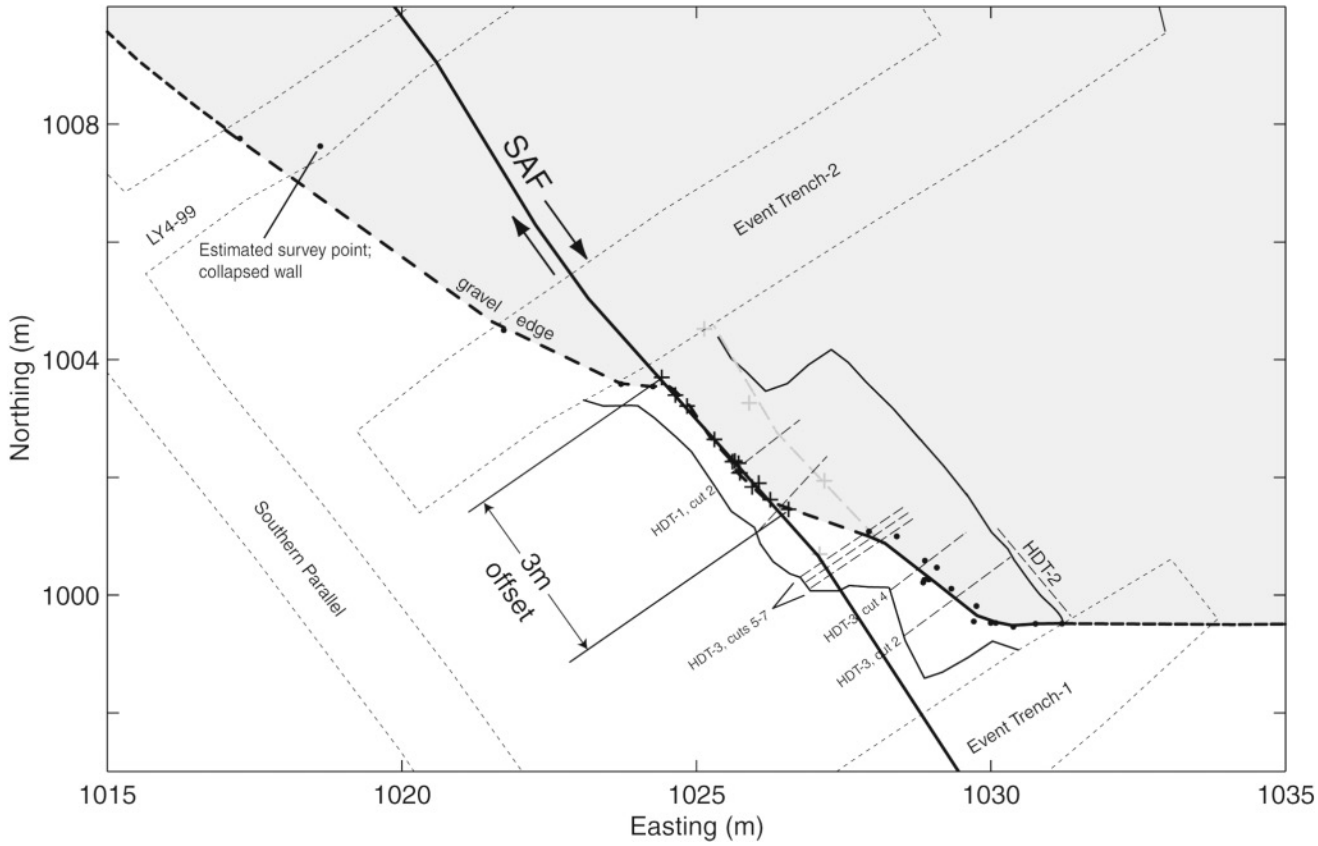

Figure 12. Plan view map of gravel edge (unit 4 shown in light gray) and fault exposed in HDTs. Black x, places where gravel edge and fault coincides; medium gray x, fault zone; black dots and heavy dashed, gravel edge; solid line, SAF. The northeastern fracture zone does not offset unit 2b-1, 2c, 4, and 5 but does separate unit 5 in cut 7. The offset is indicated by the faulted gravel edge and the abrupt change in orientation of the contact edge as defined in the successive trenches shown in Figure 8.

quently provided a somewhat sharpened edge at the toe of the flow. An alternative explanation could be that the alluvial fan did not gradationally thin toward the toe but still provided a sharpened edge with adjacent and overlying sediments. In the main fault zone trace, unit 4 exhibits rotated and heavily fractured clasts and is discontinuous across the fault. Units $2b_1$ and 2c are identifiable in the hand-excavated trenches and are also discontinuous across the fault. The marker unit 2a is distinctive in all of the hand-dug trenches. Like the adjacent fault perpendicular trenches (ET1 and ET2), the upper 40 cm contain historic, light beige, fine sand and silt (units 1a–c).

HDT-1 (Fig. 8A) was excavated perpendicular to the fault zone, on the north side of the HDT excavation area (Fig. 12). In HDT-1, the fault zone is recognized by the shearing of unit 5, rotation of clasts from unit 4, and vertical displacement of both units (Fig. 8A). The second HDT was excavated parallel to the fault and connected to ET1 (Fig. 12). The edge the alluvial fan was recognized by the contact between angular coarse pebble gravel and coarse sand (Fig. 8B). The third series of cuts (HDT-3) were made from the south side of the hand-dug trench area and perpendicular to the fault zone (Fig. 12). The alluvial fan edge was gradational in cuts 5 and 6 of Fig. 8f, g and sharper in cuts 2 and 3 (Fig. 8C, D). The fault zone was intercepted in cut 7 (Fig. 8E) and is recognized by shearing, fracturing, and displacement of units $2b_1$, 2c, 4, and 5. A secondary fracture was intercepted in cut 7 but not cut 6 of HDT-3 (Fig. 12). The secondary fracture was initially identified in ET2 but did not extend to ET1 (Figs. 4, 6). In the HDTs, the secondary fracture does not appear to cut units $2b_1$, 2c, 4, and 5, but does separate unit 5 in cut 7 (Fig. 8E).

The contact between the fault zone and the alluvial fan edge is characterized by severely fractured and rotated clasts, shearing of fine-grained sediments, and the displacement, separation, and fracturing of units 4 and 5. The contact is also identified by the absence of gravel on the west side of the fault zone. The fault zone and the gravel edge coincide for ~3.0 m, indicating ~3 m of displacement (Fig. 12). Points marking the fracture locations, gravel edge, and faulted gravel edge were surveyed with the total station in the site coordinate system and are plotted in Figure 12. Taking into account these uncertainties, we assigned an error of ± 0.70 cm. The gravel edge and fault zone contact near the

southern portion of the fan deposit surface was not distinctly defined for approximately 20–25 cm, and the lateral variation in defining the alluvial fan edge ranged from a couple of centimeters to approximately 45 cm wide.

Discussion

Our data provide additional constraints on earthquake rupture scenarios for central California and increase our understanding of the interaction among the Cholame, Parkfield, and Carrizo segments. For the Cholame segment, the Working Group on California Earthquake Probabilities (WGCEP) (1988) estimated that the recurrence interval along the Cholame is ~140 years. This estimate is based only on slip during the last event (1857) and an assumed average slip rate of 34 ± 5 mm/yr. Very little or no slip has occurred along the Cholame segment since the 1857 earthquake (Lienkaemper and Prescott, 1989), and the amount of coseismic slip that occurred is poorly constrained (e.g., Arrowsmith *et al.*, 1997; and Runnerstrom *et al.*, 2002). This study provides well-needed recurrence and offset data for this poorly characterized segment (Figs. 13, 14).

Recurrence Interval

There have only been two ground-rupturing events recorded since the deposition of unit 13, which has a 2σ calibrated age range of A.D. 1030–1300. Therefore, the maximum time between earthquakes is ~410 years, and the minimum recurrence time is 290 years, based on the interpretation of two ground-rupturing events, the time of the last one (1857), and the age of unit 13. Although the time between earthquakes is poorly constrained, it suggests that the Cholame segment does not rupture more frequently than the Carrizo segment, contrary to hypotheses by Arrowsmith *et al.* (1997), Sieh and Jahns (1984), and Harris and Archuleta (1988). However, low sedimentation rates and bioturbation may limit preservation of evidence for additional earthquakes, leading to a discrepancy in the number of earthquakes interpreted from the trenches and those that actually occurred at the site.

Displacement Data

Sieh (1978) estimated approximately 3.5 m of displacement during the 1857 earthquake based on an offset channel located 4 km northwest of our site. Alternatively, Lienkaemper and Sturm (1984) and Lienkaemper (2001) estimated approximately 5–6 m offset of this channel from the 1857 earthquake. The 3.0 ± 0.70 m of displacement measured during this study that likely records 1857 offset is consistent with the displacement estimated by Sieh (1978) (Fig. 13). However, the difference in the amount of slip recorded at our site and inferred by Lienkaemper and Sturm (1984) and Lienkaemper (2001) may be explained by either spatial slip variation along the fault or distributed slip along an adjacent strand (Fig. 2). The latter is unlikely based on geologic and geomorphic data that indicate that the fault strand adjacent to our site is not active (Stone, 1999; Stone *et al.*, 2002). However, we cannot disqualify the possibility of relatively small amounts of offset along this older strand.

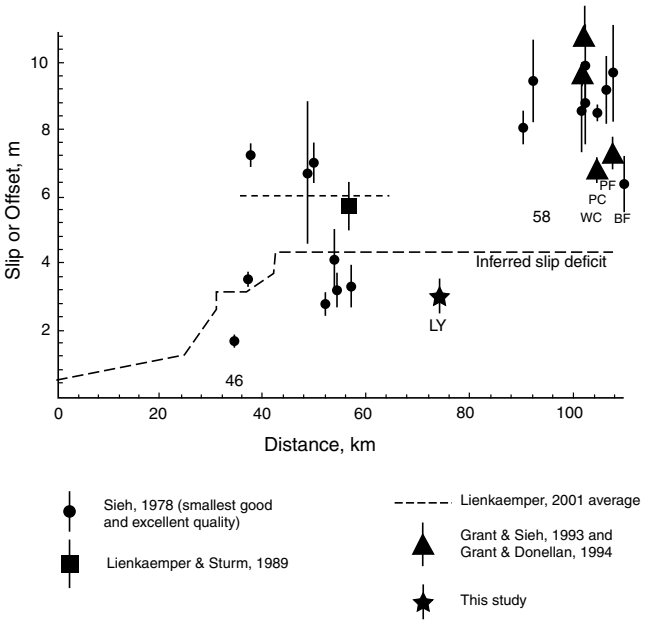

Figure 13. Inferred slip deficit and geomorphic land survey offset observations along the SAF in the area of the Cholame segment (modified from Arrowsmith *et al.*, 1997). The dashed line shows the inferred historic slip deficit assuming that all slip was released in the 1857 earthquake and that the deficit accumulates at the long-term slip rate of 35 mm/yr. The slip deficit in the north is diminished because of post-1857 fault creep and Parkfield earthquakes. Geomorphic observations of offset landforms (with attribution below and inferred to be related to the last earthquake by the various observers) are indicated with error bars. The largest displacement measurement from Grant and Donnellan (1994) was measured over a 1-mile-wide aperture and may represent fault slip and distributed deformation. Note also that Runnerstrom *et al.* (2002) suggested that deeper slip along the SAF about 7 km northwest of the LY site may have been up to 17.5 m. The star indicates the offset determined in this study. 46 and 58 show the locations where the SAF crosses State Highways 46 and 58 and effectively bound the Cholame segment. Wallace Creek (WC), Phelan Creeks (PC), Phelan Fan (PF), Bidart Fan (BF), and Las Yeguas (LY) are the major earthquake geology study sites in the region. Distance is measured southeast along the SAF from Claassen at the northwest end of the Parkfield segment.

The 3.0 ± 0.70 m of offset from the 1857 earthquake measured during this study is 2–3 times less and nearly 3 times more than that measured in the adjacent Carrizo and Parkfield segments to the south and north, respectively (Sieh, 1978; Sieh and Jahns, 1984; Grant and Sieh, 1993; Grant and Donnellan, 1994). The large difference in slip between the Carrizo and our site indicate that there may be some fundamental difference in fault properties between the two areas, which is not easily explained by lower prestressing along the Cholame prior to the 1857 event (Hilley *et al.*,

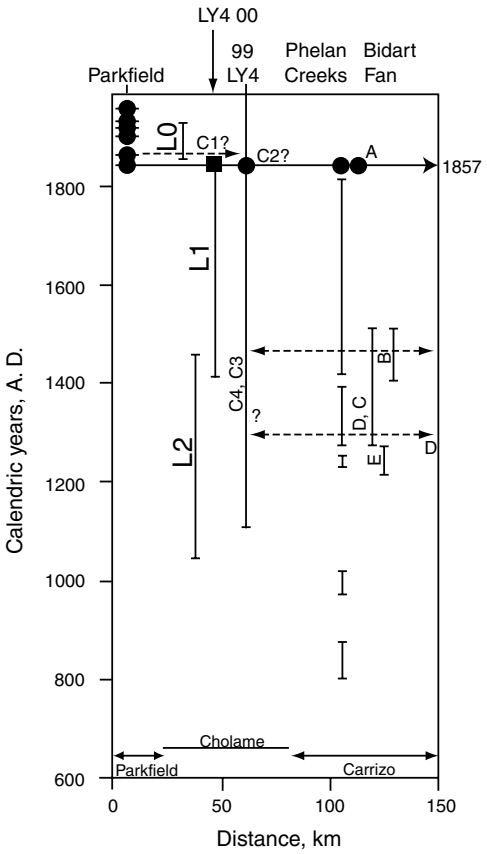

Figure 14. Event correlation diagram for the northern Carrizo, Cholame, and Parkfield segments of the SAF. This chart compares earthquake chronologies from Bidart Fan (Grant and Sieh, 1994), Phelan Creeks (J. D. Sims, personal comm.), LY4-99 (Stone *et al.*, 2002), the historic Parkfield record (e.g., Bakun, and Lindh, 1985b), and this study. L2 could be correlative to the penultimate Carrizo event (event B) that likely occurred within the period A.D. 1405–1510 (Grant and Sieh, 1994). If event L2 and L1 are the same event, then they would represent the 1857 earthquake event horizon. If event L2 and L1 are not the same event, then L1 is likely the 1857 event, L2 would be correlative to the penultimate Carrizo event B and to either C or D Carrizo events (Grant and Sieh, 1994). Event L0, the ground-shaking event, could be correlative to a post-1857 Parkfield event.

2001). Continued paleoseismic investigations that clarify 1857 and older offsets will help resolve these potential differences.

Correlation of Events

We tentatively correlate the oldest event at our site to one with a similar age further south in the Carrizo Plain (Fig. 14). The age of unit 13, A.D. 1030–1300 and the subsequent soil development above that unit could indicate a time lapse of about 150 to 300 years before event L2 occurred. The L2 event could be correlative with the penultimate Carrizo (event B) that likely occurred after a date within the range 1405–1510 A.D. or the Carrizo event C (Grant and Sieh, 1994). Event L1 is correlative to the 1857 Fort Tejon earthquake. Event L0, the fracturing event, could be correlative to a post-1857 Parkfield event, such as the 1877 or 1881 earthquakes (Toppozada, 2002). If regional seismicity was enhanced following the earthquake of 1857 (Toppozada, 2000), then it is plausible that aseismic creep or triggered slip from an older Parkfield event could have resulted in fracturing at the LY4 site in the decades following 1857. Although the events we infer from the LY4 site have poor age constraints for event correlation, the results are inconsistent with the higher rupture frequency and lower magnitude hypotheses for Cholame earthquake recurrence of WGCEP (1988), Arrowsmith *et al.* (1997), Harris and Archuleta (1988), and Sieh and Jahns (1984).

Comparison of Recent Results to Previous Work at the LY4 Site

A prior paleoseismic study at the LY4 site (Stone *et al.*, 2002) identified two to four surface ruptures at the site since A.D. 1058–1291 and provided evidence suggestive of post-1857 displacement. The investigations made during our study attempted to measure displacement across the fault, corroborate evidence for a post-1857 ground-rupturing event, and provide better age control and corroboration of the ruptures interpreted by Stone *et al.* (2002). We did not confirm a post-1857 ground-rupturing event but did identify post-1857 tectonic fractures that cut historic sediments. The origin of these structures is enigmatic but do not appear to represent major coseismic surface rupture at LY4. Our event L1 is correlative to an event (C2 or C1/C2) in the Stone *et al.* (2002) study, both of which represent the 1857 earthquake. Differences in event timing results from different sedimentologic interpretations. The Stone *et al.* (2002) study interprets unit 2b (unit 100) as a massive debris flow that retained its original depositional texture. Historic exotic pollen grains were found in a sample taken from this unit by Stone *et al.* (2002) resulting in a post-1873 age estimate for the sediments. They cite fracturing and lateral thinning of unit 2b (unit 100) as evidence for a post-1873 ground-rupturing event. We interpret unit 2b as a densely bioturbated sandy silt that has been thoroughly mixed, thus combining younger overlying sediments with those sampled for pollen analysis. We suggest that the lateral thinning was the result of the 1857 earthquake. Although the fractures observed in the Stone *et al.* (2002) study do not cut historic sediments, they could be from the 1857 event or the L0 event in this study. C3 event of Stone *et al.* (2002) matches the oldest event observed during this study, L2. They also interpreted two pre-1857 ground-rupturing events. However, we only identified a single pre-1857 earthquake because of stratigraphic limitations.

Conclusions

Paleoseismic investigations at the LY4 site provide better constraints on the number of earthquakes along the Cholame segment of the SAF and the lateral displacement from the 1857 earthquake. We identified two ground-rupturing earthquakes, the oldest occurring after a date within the range A.D. 1030–1300 and the youngest being the 1857 Fort Tejon earthquake. This rate of occurrence of earthquakes is lower than previously expected but is consistent with earlier preliminary paleoseismic results (Stone *et al.*, 2002). Three-dimensional exposure of an alluvial fan revealed 3.0 ± 0.7 m of on-fault surface offset from the 1857 event. Evidence for post-1857 tectonic fracturing of historic sediments may have resulted from creep, triggered slip, or ground shaking from nearby moderate earthquakes.

Acknowledgments

We thank Darrell and Nola Twisselman and Joe Sill for permission to excavate and live on their property. We would also like to recognize the helpfulness and hospitality of the entire Twisselman family. Field help was donated by Scott Nowicki, Jen Lewicki, Matt Baillie, Valerio Lombardo, Brian Gootee, Erin Young, and Lee Amoroso. J. Young extends exceptional gratitude to G. Hilley for his detailed review and helpful commentary. We thank T. Fumal, J. Lienkaemper, D. Schwartz, G. Sietz, H. Stenner, and T. Rockwell for their helpful field review and discussions. We thank Dallas Rhodes for insightful geomorphologic discussions. Manfred Strecker helped with valuable aid for the final review of our work, and we acknowledge support by the IQN Potsdam (DAAD) granted to the Department of Geosciences of Potsdam University, Germany. This work is supported by the Southern California Earthquake Center (SCEC). SCEC is funded by the National Science Foundation Cooperative Agreement EAR-8920136 and U.S. Geological Survey Cooperative Agreements 14-08-0001-A0899 and 1434-HQ-97AG01718. The SCEC Contribution Number for this article is 581.

References

Arrowsmith, R., K. McNally and J. Davis (1997). Potential for earthquake rupture and M 7 earthquakes along the Parkfield, Cholame, and Carrizo segments of the San Andreas Fault, *Seism. Res. Lett.* **68,** 902–916.

Bakun, W. H., and A. G. Lindh (1985a). The Parkfield, California, earthquake prediction experiment, in *Minutes of the National Earthquake Prediction Evaluation Council, July 26–27, Menlo Park, California, C. F. Shearer (Editor), U.S. Geol. Surv. Open-File Rep.* 32–38.

Bakun, W. H., and A. G. Lindh (1985b). The Parkfield, California, earthquake prediction experiment, *Science* **229,** 619–624.

Dibblee, T. W., Jr. (1973). Regional geologic map of San Andreas and related faults in Carrizo Plain, Temblor, Caliente, and La Panza ranges and vicinity, California, U.S. Geol. Surv. Misc. Geol. Invest. Map, scale 1:125,000, p. 9.

Eichel, M. H. (1971). The Carrizo Plain: a geographic study of settlement, land use and change, *M.S. Thesis*, San Jose State College, San Jose, California, p. 71.

Grant, L. B., and A. Donnellan (1994). 1855 and 1991 Surveys of the San Andreas fault: implications for fault mechanics, *Bull. Seism. Soc. Am.* **84,** 241–246.

Grant, L. B., and K. Sieh (1993). Stratigraphic evidence for seven meters of dextral slip on the San Andreas Fault during the 1857 earthquake in the Carrizo Plain, *Bull. Seism. Soc. Am.* **83,** 619–635.

Grant, L. B., and K. Sieh (1994). Paleoseismic evidence of clustered earthquakes on the San Andreas fault in the Carrizo Plain, California, *J. Geophys. Res.* **99,** B4, 6819–6841.

Harris, R. A., and R. J. Archuleta (1988). Slip deficit on the San Andreas Fault: potential for a magnitude 7 event at Parkfield, in *AGU 1987 Fall Meeting Abstracts: EOS Transactions*, American Geophysical Union, Washington, D.C., p. 1350.

Hilley, G. E., J. R. Arrowsmith, and E. M. Stone (2001). Using microseismicity and surface offset data to define fault segment boundaries along low friction faults, with an example from the Cholame–Carrizo segment boundary along the San Andreas Fault, Southern California, *Bull. Seism. Soc. Am.* **91,** 427–440.

Lienkaemper, J. J. (2001). 1857 Slip on the San Andreas fault southeast of Cholame, *Bull. Seism. Soc. Am.* **91,** no. 6, 1659–1672.

Lienkaemper, J. J., and W. H. Prescott (1984). Historic surface slip along the San Andreas fault near Parkfield, California, *J. Geophys. Res.* **94,** 17,647–17,670.

Lienkaemper, J., and T. A. Sturm (1989). Reconstruction of a channel offset in 1857 (?) by the San Andreas Fault near Cholame, California, *Bull. Seism. Soc. Am.* **79,** 901–909.

Ramsey C. B. (1995). Radiocarbon calibration and analysis of stratigraphy: the OxCal Program, *Radiocarbon* **37,** no. 2, 425–430.

Runnerstrom, E. E., L. B. Grant, J R. Arrowsmith, D. D. Rhodes, and E. M. Stone (2002). Displacement across the Cholame segment of the San Andreas fault between 1855 and 1893 from cadastral surveys, *Bull. Seism. Soc. Am.* **92,** no. 7, 2659–2669.

Schwartz, D. P., and K. J. Coppersmith (1986). Seismic hazards; new trends in analysis using geologic data, in *Active Tectonics*, R. E. Wallace (Editor), National Academy Press, Washington, D.C., 215–230.

Sieh, K. E. (1978). Slip along the San Andreas fault associated with the great 1857 earthquake, *Bull. Seism. Soc. Am.* **68,** 1731–1749.

Sieh, K. E., and R. H. Jahns (1984). Holocene activity of the San Andreas Fault at Wallace Creek, California, *Geol. Soc. Am. Bull.* **95,** 883–896.

Stone, E. M. (1999). Geomorphology, structure and paleoseismology of the central Cholame segment, Carrizo Plain, California, *M.S. Thesis*, Arizona State University, Tempe, 100 pp.

Stone, E., L. B. Grant, and J R. Arrowsmith (2002). Recent rupture history of the San Andreas fault southeast of Cholame in the northern Carrizo Plain, California, *Bull. Seism. Soc. Am.* **92,** no. 3, 983–997.

Toppozada, T., D. Branum, M. Petersen, C. Hallstrom, and M. Reichle (2000). Epicenters of and areas damaged by M ≥ 5.5 California earthquakes, 1800–1999, Calif. Div. Mines Geol. Map Sheet 49, scale 1:5,000,000.

Toppozada, T., D. Branum, M. Reichle, and C. Hallstrom (2002). San Andreas fault zone, California: *M* ≥5.5 earthquake history, *Bull. Seism. Soc. Am.* **92,** no. 7, 2555–2601.

Trumbore, S. E. (1998). *Radiocarbon Geochronology in Dating and Earthquakes: Review of Quaternary Geochronology and Its Application to Paleoseismology*, J. M. Sowers, J. S. Noller, and W. R. Lettis (Editors): Division of Engineering Technology, Office of Nuclear Regulatory Research, U.S. Nuclear Regulatory Commission, Washington, D.C., 2-69–2-99.

Vedder J. G., and R. E. Wallace (1970). Map showing recently active breaks along the San Andreas and related faults between Cholame Valley and Tejon Pass, CA, U.S. Geol. Surv. Misc. Geologic Invest. Map I-574, scale 1-24,000.

Working Group on California Earthquake Probabilities (WGCEP) (1988). Probabilities of large earthquakes occurring in California on the San Andreas Fault, *U.S. Geol. Surv. Open-File Rep. OFR 88–398*, 62 pp.

Wood, W. R., and Johnson, D. L., (1978). A survey of disturbance processes in archaeological site formation, *Adv. Archeol. Meth. Theory*, **1,** 315–381.

Department of Geological Sciences
Arizona State University
P.O. Box 1404
Tempe, Arizona 82587-1404
jeri.young@asu.edu; ramon.Arrowsmith@asu.edu; bgootee@asu.edu
(J.J.Y., J R.A., B.G.)

Istituto Nazionale di Geofisica e Vulcanologia
Via di Vigna Murata 605
00143, Rome, Italy
colini@ingv.it
(L.C.)

Department of Environmental Analysis and Design and Analysis
University of California, Irvine
Irvine, California 92697-7070
lgrant@uci.edu
(L.B.G.)

Manuscript received 14 May 2001.